Absolute calibration of LIDAR Thomson scattering systems by rotational Raman scattering

R. Scannell,[1,a)] M. Beurskens,[1] M. Kempenaars,[1] G. Naylor,[1] M. Walsh,[2] T. O'Gorman,[3] and R. Pasqualotto[4]
[1]*EURATOM/CCFE Fusion Association, Culham Science Centre, Abingdon OX14 3DB, United Kingdom*
[2]*CHD Department, Diagnostics Division, ITER Organisation, Cadarache, 13106 St. Paul-lez-Durance, France*
[3]*Department of Electrical and Electronic Engineering, University College Cork, Cork, Ireland*
[4]*Consorzio RFX-Associazione Euratom-Enea sulla Fusione, Corso Stati Uniti 4, I-35127 Padova, Italy*

(Received 9 February 2010; accepted 5 March 2010; published online 21 April 2010)

Absolute calibration of LIDAR Thomson scattering systems on large fusion devices may be achieved using rotational Raman scattering. The choice of calibrating gas molecule presents different options and design trade-offs and is likely to be strongly dependent on the laser wavelength selected. Raman scattering of hydrogenic molecules produces a very broad spectrum, however, with far fewer scattered photons than scattering from nitrogen or oxygen at the same gas pressure. Lower laser wavelengths have the advantage that the Raman cross section increases, $\sigma_{\mathrm{Raman}} \propto 1/\lambda_0^4$, but the disadvantage that the spectral width of the scattered spectrum decreases, $\Delta\lambda_{\mathrm{Raman}} \propto \lambda_0^2$. This narrower spectrum makes measurement closer to the laser wavelength necessary. The design of the calibration technique presents a number of challenges. Some of these challenges are generic to all Thomson scattering systems. These include detecting a sufficient number of photoelectrons and designing filters that measure close to the laser wavelength while simultaneously achieving adequate blocking of the laser wavelength. An issue specific to LIDAR systems arises since the collection optics operates over a wide range of depth of field. This wide depth of field has the effect of changing the angle of light incident on the optical interference filter with plasma major radius. The angular distribution then determines the effective spectral transmission function of the interference filter and hence impacts on the accuracy of the absolute calibration. One method that can be used to increase absolute calibration accuracy is collecting both Stokes and anti-Stokes lines with optical filter transmission bands specifically designed to reduce systematic uncertainty. © *2010 American Institute of Physics.* [doi:10.1063/1.3374111]

I. INTRODUCTION

LIDAR Thomson scattering systems are required to accurately measure radial electron density profiles in fusion plasmas. One widely used technique for absolute calibration of Thomson scattering measurements is Raman scattering from a known pressure of hydrogen or nitrogen gas.[1,2] A core LIDAR system is planned for ITER. Potential designs for this system are outlined in Ref. 3. The performance of one such system based on a 1064 nm laser is analyzed in Ref. 4. The aim of this paper is to look at some of the generic issues of Raman calibration faced on large fusion devices. Aspects of the proposed ITER design are used to illustrate a number of these issues.

The laser wavelength is determined by the design requirements of the Thomson scattering system. Using this laser wavelength, different permutations of calibrating gas and optical filters will be considered to obtain the best calibration design solution. The filter wavelength ranges determined from this design solution must be compatible with the requirements for Thomson scattering measurements.

Accurate Raman calibration requires accurate spectral calibration of the spectrometer, possibly as a function of measurement solid angle, and to a lesser extent accurate measurement of the gas temperature of the calibrating molecule. The engineering constraints of the vessel must also be considered. While it is possible to put 150 mbar of calibrating gas into smaller tokamaks, this is not always possible on large devices due to interaction with cryopumping and cooled components. At low pressure the overall number of collected scattered photons may limit the feasibility of certain calibration techniques.

While this paper examines the use of Raman scattering to provide the absolute calibration, another possibility for absolute calibration is Rayleigh scattering. Both techniques are examined for a conventional geometry system in Ref. 2. Rayleigh calibration has the disadvantage that it is subject to stray laser light and requires an optical filter at the laser wavelength, which cannot be used for Thomson scattering. Certain TS (Thomson scattering) system designs use crystals to absorb light at the laser wavelength and hence exclude the possibility of Rayleigh calibration.[1]

II. LASER SYSTEMS

The two LIDAR systems on JET are both based on individual lasers.[5] However, as originally proposed in Ref. 6, two lasers of different wavelengths could be used in a single LIDAR system. The main purpose of the additional laser could be to measure more accurately in a certain electron

a)Electronic mail: rory.scannell@ccfe.ac.uk.

temperature range or to operate as an auxiliary laser to aid the spectral or absolute calibration of the primary laser. Ideally both lasers would have independent absolute calibrations; alternatively the absolute calibration obtained from one laser could be used to calibrate the other laser system.

For the purposes of this paper only two laser wavelengths, 1064 and 532 nm, are examined in detail. These were chosen because they are at the extremes of the wavelength range of lasers that would be considered for LIDAR systems. For an intermediate wavelength laser, such as the Ruby laser used on either of the JET systems,[5,7] the conclusions drawn would be somewhere between those for the 532 and 1064 nm lasers.

The 1064 nm laser considered is assumed to be able to inject 2.5 J of energy per pulse into the plasma. If this laser is frequency doubled, up to approximately half of the energy can be converted to 532 nm; the other half of the energy remains at 1064 nm. The number of photons in the 532 nm pulse is reduced by a further factor of two since the energy per photon is twice as high at 532 nm. Simply put, for every four photons a 1064 nm laser fires into the plasma, a 532 nm laser fires in one. The 532 nm laser is readily commercially available at low cost and would fit in well with a bank of 1064 nm lasers in a two wavelength LIDAR system.

III. RAMAN CALIBRATION LASER WAVELENGTH

A Thomson scattering system can be calibrated in nitrogen, oxygen, hydrogen, or deuterium depending on which gases are allowed in the vacuum vessel. Currently the technology for detectors in the visible regions is available.[8] Detectors are also available in the infrared region but have relatively poor effective quantum efficiency (EQE). For a 1064 nm laser, detectors in the visible region will allow measurement of Thomson scattered light for a broad range of electron temperatures, but currently only low EQE detectors can detect Raman scattered light. Frequency doubling a 1064 nm laser would allow the high EQE detectors to detect the Raman scattering from the 532 nm laser pulse. This Raman scattering from the 532 nm pulse could be used to provide an absolute density calibration that could be scaled to the 1064 nm laser system.

The Raman cross section scales with laser wavelength λ_0 as[9]

$$\sigma_{\mathrm{Raman}} \propto \frac{1}{\lambda_0^4}, \tag{1}$$

and hence there is 16 times more Raman scattered light from a 532 nm laser than from a 1064 nm laser of equivalent energy. Due to this strong scaling of scattered light with laser wavelength, absolute calibration from a 532 nm laser will remain an attractive option even if high EQE fast infrared detectors are developed. A similar scaling of cross section occurs for Rayleigh scattering.

At lower laser wavelength the separation between Raman lines decreases. The wavelength of the Raman line resulting from the $j \rightarrow j-2$ transition[10] is in general given by

$$\lambda_{j\rightarrow j-2} = \frac{1}{\frac{1}{\lambda_0} + B_0(4J-2)} \quad \text{for} \quad j = 2,3,\ldots \tag{2}$$

which may be approximated as in Ref. 11 using a Taylor series expansion to

$$\lambda_{j\rightarrow j-2} \approx \lambda_0 - \lambda_0^2 B_0(4J-2), \tag{3}$$

where B_0 is the rotational constant,[2,9,10,12] which is 198.96 m^{-1} in N_2, 143.8 m^{-1} in O_2, 2991.05 m^{-1} in D_2, and 5933.9 m^{-1} in H_2. The gap between subsequent Raman lines $\Delta\lambda = \lambda_{j+1\rightarrow j-1} - \lambda_{j\rightarrow j-2}$ is given by

$$\Delta\lambda \approx -4B_0\lambda_0^2, \tag{4}$$

which for nitrogen and oxygen evaluates to $\Delta\lambda = 0.6-0.9$ nm for a scattering wavelength of 1064 nm and $\Delta\lambda = 0.15-0.25$ nm for a scattering wavelength of 532 nm. For this reason, the Raman scattered lines from a 532 nm laser are quite close to the laser wavelength. Optical filters must have good transmission to within 2–3 nm of the laser wavelength to detect this spectrum, while at the same time good blocking at the laser wavelength. The spectral broadening of the laser wavelength should be small since it would have a significant effect on the integrated Raman cross section in a spectral channel.

IV. RAMAN CALIBRATION GAS

Raman calibration in H_2 or D_2 gas[13] overcomes the difficulty of proximity to the laser wavelength and reduces the strong dependency of calibration accuracy on the accuracy of the filter transmission function. This is a strong advantage since the optical filter transmission will vary across the plasma. A further advantage of calibration using a hydrogenic molecule is that broadening of Raman lines due to nonmonochromatic laser pulses will not affect the cross section since the lines are not at the edge of the filter.

There are fewer spectral lines for hydrogenic molecules. There are four strong Stokes lines corresponding to transitions $j=0\rightarrow 2$, $j=1\rightarrow 3$, $j=2\rightarrow 4$, and $j=3\rightarrow 5$. There are two strong anti-Stokes lines corresponding to the transitions $j=3\rightarrow 1$ and $j=2\rightarrow 0$. The intensities of odd and even lines reverse in H_2 and D_2 due to their different nuclear spin orientations.[14] Due to the smaller number of lines a much lower number of scattered photons are detected for the equivalent gas pressure relative to Raman scattering from N_2 or O_2. A practical consideration is that hydrogenic gases are explosive in reaction with air and so may pose a safety risk, which translates to a low allowable pressure. It is likely that the ITER vacuum vessel will be designed to cope with of the order of 10 mbar of hydrogen gas from regeneration of the cryopumps, and so it should be possible to fill with this pressure of hydrogen for the purposes of Raman scattering.

The total number of detected photoelectrons from Raman scattering, integrated over the entire spectrum, at a gas pressure of 10 mbar for a variety of molecules and laser wavelengths are given in Table I. It is important to note that an EQE of 4% at all wavelengths was used to compile Table I. This EQE is easily achievable at lower wavelengths but

TABLE I. Total number of detected photoelectrons from Raman scattering integrated over the entire spectrum at a gas pressure of 10 mbar. Optical transmission of 10%, f/12, scattering length of 67 mm, and EQE of 4%.

	H_2	D_2	N_2	O_2
1.25 J, λ_0=532 nm	124	141	836	2135
3.0 J, λ_0=694.3 nm	129	151	902	2303
2.5 J, λ_0=1064 nm	28	34	208	536

not necessarily in the infrared. The possible detectors available for the ITER LIDAR system, and their EQE are discussed in detail in Ref. 8. 10 mbar is a low gas pressure and so should be acceptable from a safety perspective. If a higher gas pressure is allowable, the number of scattered photons may be scaled linearly. The table shows that there are significantly more scattered photons from the high Z elements and significantly more scattered photons from the lower wavelength lasers. The table also shows that scattering from 10 mbar of nitrogen using a 1064 nm laser produces a similar number of photons as scattering from 10 mbar of hydrogen using a 532 nm laser. This number of photons is measurable; scattering from 10 mbar of nitrogen is routinely performed on MAST.[15] Although in the MAST case this is achieved with higher etendue collection optics, it is performed with lower laser energy and much shorter scattering length than the system used to compile Table I. The spectral distributions of the scattered photons for the different gases and lasers are shown in Fig. 1. Oxygen provides a greater number of scattered photons than nitrogen, although both elements produce scattered spectra close to the laser wavelength. To obtain a random error of less than 1%, at least 10 000 photo electrons should be detected from Raman scattering at each gas pressure. The number of laser pulses required to achieve this accuracy at the center of plasma may be deduced from Table I.

V. FILTER WAVELENGTHS FOR RAMAN SCATTERING

Four different filter transmission bands are considered in detail in the following sections of this paper. These transmission bands are summarized in Fig. 2(a). To capture nitrogen anti-Stokes lines from a 1064 nm laser, a filter of bandwidth 20 nm transmitting from 1041.5–1061.5 nm was chosen. This filter will capture a very large fraction of the anti-Stokes spectrum, missing only those lines very close to the laser wavelength. As shown in Fig. 2(b), this filter will provide useful Thomson scattering measurements down to low electron temperature.

The filter considered for capturing nitrogen Stokes lines from a 1064 nm laser is also 20 nm and transmits from 1070.25–1090.25 nm. A larger gap is required to the laser

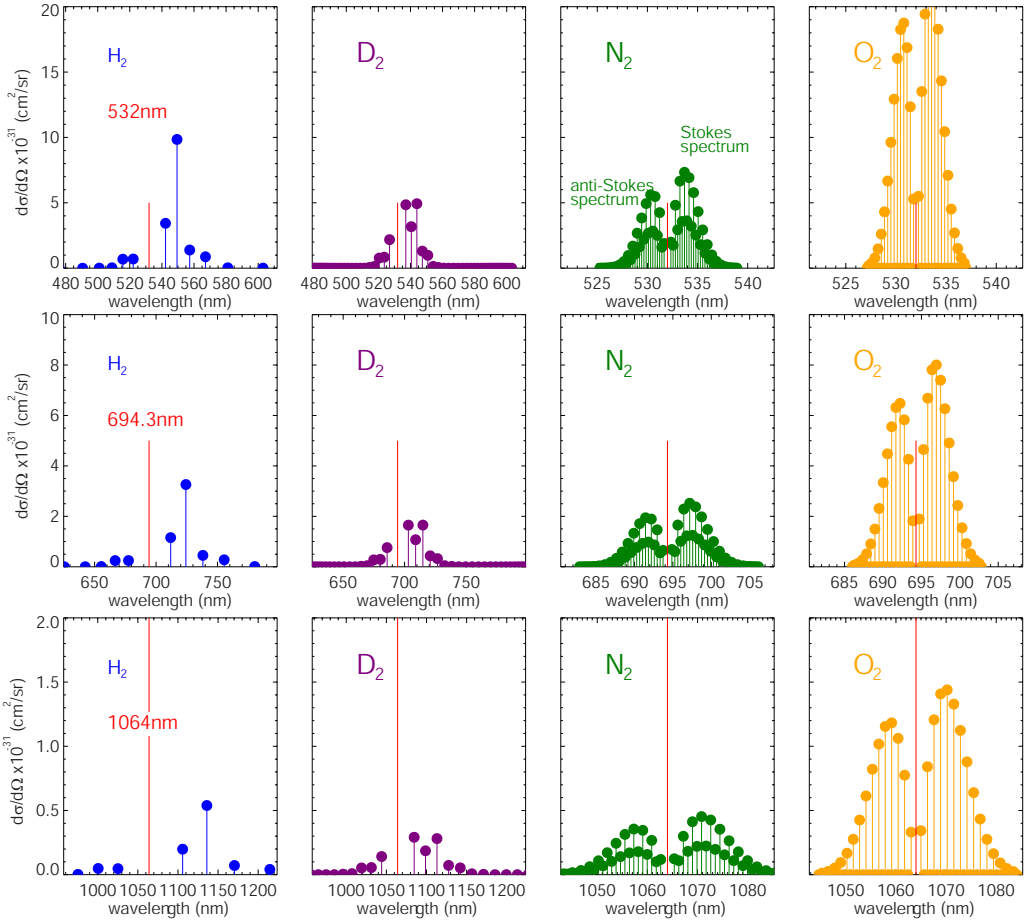

FIG. 1. (Color online) Raman spectra for scattering from various laser wavelengths and gases at 298 K. Note that each row of plots has different intensity scales.

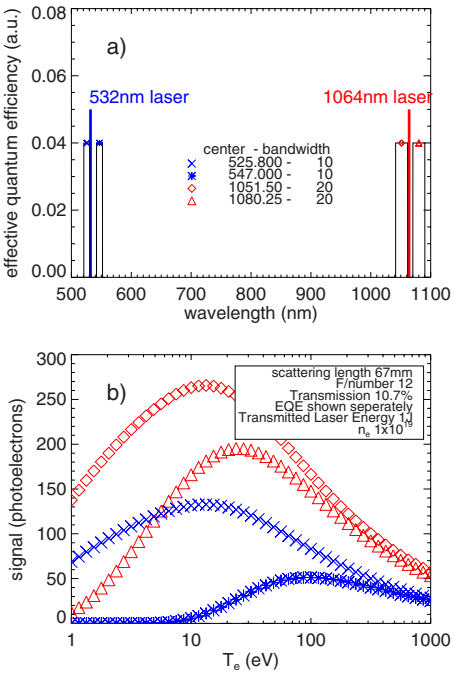

FIG. 2. (Color online) (a) Filter transmission bands considered in the following sections. (b) Scattered signal received in these channels as a function of electron temperature assuming incident rays are normal to the filter surface.

wavelength for filters above the laser wavelength since filter transmission bands will be naturally blueshifted by angular variation of light on the filter.

The filter considered to capture nitrogen anti-Stokes lines from a 532 nm laser is equivalent to the filter capturing anti-Stokes lines from a 1064 nm laser scaled by the laser wavelength. A further filter is used to examine the possibility of capturing Hydrogen Stokes lines from the 532 nm laser. This hydrogen filter transmits from 542–552 nm, which has a relatively high equivalent electron temperature compared with the nitrogen filters. This filter need not be designed specifically for Raman scattering, and any filter encompassing this wavelength band would be sufficient.

VI. WAVELENGTH SHIFT DUE TO ANGLE OF LIGHT

If the angle of light incident on an optical filter is not normal to the surface, the effective wavelength of that light as seen by the optical filter is shifted. This has the effect of broadening the spectral transmission of the filter for larger angles of incident light. In general the wavelength shift for light incident with angle θ on an optical filter of effective refractive index n_{eff} in a surrounding medium of refractive index n_0 is given by Eq. (5),

$$\lambda \rightarrow \lambda \sqrt{1 - \left(\frac{n_0}{n_{\text{eff}}}\right)^2 \sin^2 \theta}. \tag{5}$$

The polarization of the light with respect to the filter surface can influence the wavelength shift of the light. In general *s* polarized light experiences a smaller wavelength shift (has a larger effective refractive index) than *p* polarized light.

TABLE II. Five scattering centers across the major radius of the ITER plasma used to compare filter performance.

Position index	r/a	Distance from vacuum window (mm)	Collection F/#
1	+1.0	1760	6
2	+0.5	2810	9
3	0.0	3860	12
4	−0.5	4910	15
5	−1.0	5960	18

A. Angular distribution of light on filters

LIDAR collection optics has a large depth of field of light collection in the object plane of the collection optics. Because of this, the light imaged onto the optical filters in the spectrometer has a different angular distribution dependent on the major radius it originates from in the plasma. The spectrometer etendue is fixed. Conserving this etendue, the spectrometer may be designed with larger filters to reduce the angular distribution of light on the filters. The smaller the resulting angular distribution of light, the closer the filter transfer function to the ideal transfer function. The trade-off is that larger optical filters are more difficult to manufacture and require larger spectrometers to accommodate them.

To determine the size of filter required for this spectrometer, five positions along the measurement chord of the ITER LIDAR system, as shown in Fig. 1 in Ref. 3, are considered. The five positions are sequentially separated by 1.05 m, and their parameters are described in Table II. As well as considering five positions in the plasma, four different optical filter diameters are examined. The four optical filters chosen have diameters of 170, 215, 260, and 300 mm, respectively. The maximum diameter was chosen after consultation with a filter manufacturer.

The ray angles of light on the four filters from the five different positions in the plasma are shown in Fig. 3. Different spectrometer designs have been created to house the different diameter filters. As the filter size decreases, two effects may be observed. First, there is an increase in the angular distribution of the rays falling on the filter. Second, there is an increase in the mean angle of rays. For each position in the plasma and each optical filter, the ray angle distribution is calculated from 100 points taken from a random position in the field of the scattering center and traveling through a random position in the pupil of the collection optics. The distribution of rays on the filter increases with increasing F/number of collection.

B. Impact of angular shift on filter transfer functions

Once the angular distribution of light on the filter has been determined, the wavelength shift may be calculated and the effective transmission function of the filter calculated. This is examined in Fig. 3 for a normalized central wavelength $\lambda_0 = 1.0$ and filter of bandwidth $\Delta\lambda = 0.01 * \lambda_0$. The four plots on the right hand column of Fig. 3 show the effective filter transfer functions as seen from each position in the plasma for each filter diameter. Two trends are observed:

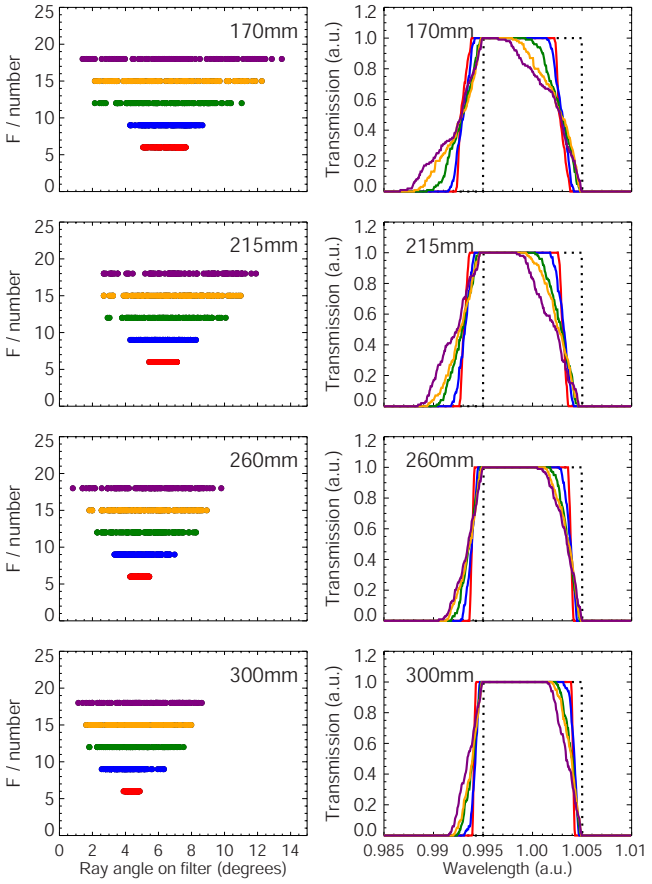

FIG. 3. (Color online) The column on the left shows the distribution of ray angles of light on the different diameters of optical filters. The column on the right shows the ideal filter transfer function (dashed line) and resulting filter transfer functions due to the angular distribution of light.

with decreasing filter diameter passbands become more blueshifted, and similarly with increasing f-number filter passbands become more blueshifted.

The filters bandwidths examined in this case are 1% of the laser wavelength; the filters for capturing nitrogen Raman lines shown in Fig. 2 are 2% of the laser wavelength. From this it may be deduced that the change in transmission function will have an effect on the measurement of electron temperature at low electron temperatures, which must be taken into account. The change in transmission function will however have a large impact on the integrated Raman cross section in each spectral channel. This will have a large impact on the electron density profile measurement.

VII. RAMAN CALIBRATION IN N_2 AT 1064 nm

The shifted filter transfer functions for a filter capturing anti-Stokes Raman lines are shown in Fig. 4 for the four filter diameters. The integrated Raman cross section for each position in the plasma and each filter diameter are also shown. There is a trend of decreasing variation in the integrated Raman cross section with increasing filter diameter. This trend is not completely linear since the integrated Raman cross section is strongly dependent on the transmission of the filters at a few very intense Raman lines. However, from this figure it is observed that to obtain variation in the

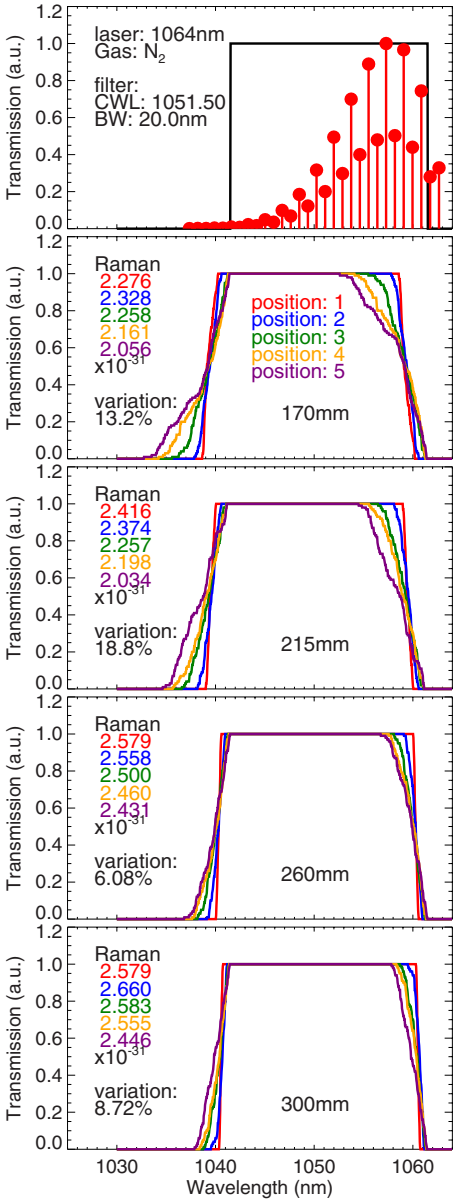

FIG. 4. (Color online) The top plot shows an underlying spectral transmission function for rays incident at 0° and the Raman spectrum for nitrogen at 300 K. The subsequent plots show the resulting spectral transmission functions and integrated Raman cross sections for filters of four different diameters from five different positions in the plasma.

integrated Raman cross section of $<10\%$, a filter diameter of at least 260 mm is required. The benefit in increasing filter size from 260 to 300 mm is relatively small.

Detecting Stokes lines is not directly equivalent to detecting anti-Stokes lines since filters detecting Stokes lines must have larger clearance from the laser wavelength. This larger clearance is required to prevent transmission of stray laser light. Transmission at the laser wavelength of no more than 0.001%, that is, blocking of optical density 5, is desirable. The clearance required is examined in Fig. 5. To illustrate the clearance, the lower passband of the filter was estimated by determining the lowest wavelength with a transmission of 1%. There should be a number of nanometers gap between this lower passband and the laser wavelength. In Fig. 5, it is shown that the shift of the lower passband is

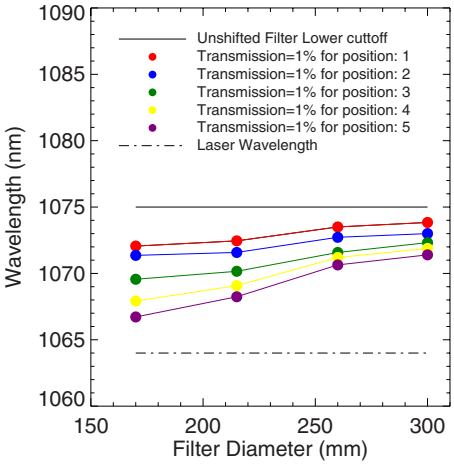

FIG. 5. (Color online) This shows the shift in the lower passband for a variety of filter diameters and positions in the plasma. The *ideal* case is for rays incident normal to the filter only. The lower passband is defined as the lowest wavelength where the shifted filter transmission exceeds 1%.

$<\approx 4$ nm for filters of widths 260 and 300 mm but is $>\approx 7$ nm for filters of widths 215 and 170 mm. Hence, it would be possible to design filters to capture a large fraction of the Stokes spectrum with filters of at least 260 mm diameter but not possible with smaller diameter filters due to the wavelength gap required.

VIII. COMBINATION OF STOKES AND ANTI-STOKES

A higher level of calibration accuracy may be obtained by using the information from both Stokes and anti-Stokes lines. Figure 6 shows a specific case of capturing both sets of lines. The left-hand figure contains both the Stokes and anti-Stokes spectrum as well as the ideal filter transfer functions that would be used to capture these spectra. As scattering centers further into the plasma are examined, there is an increase in the angle of light on the optical filters. Due to the increase in angle of light, both the Stokes and anti-Stokes filters move to lower wavelength. Moving to lower wavelength increases the Raman scattered signal collected in the Stokes filter and decreases the signal in the anti-Stokes filter. However, the sum of the anti-Stokes and Stokes signal remains relatively constant irrespective of the position the scattered signal is collected from in the plasma as the increase in

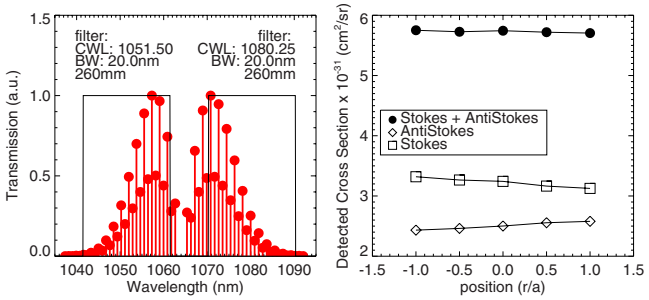

FIG. 6. (Color online) The above figure shows the spectrum of both Stokes and anti-Stokes scattered light from Raman scattering from nitrogen using a 1064 nm laser. The ideal filter transfer functions used to capture the Stokes and anti-Stokes lines are also shown. The integrated Raman cross sections for anti-Stokes, Stokes, and their sum are shown on the figure to the right.

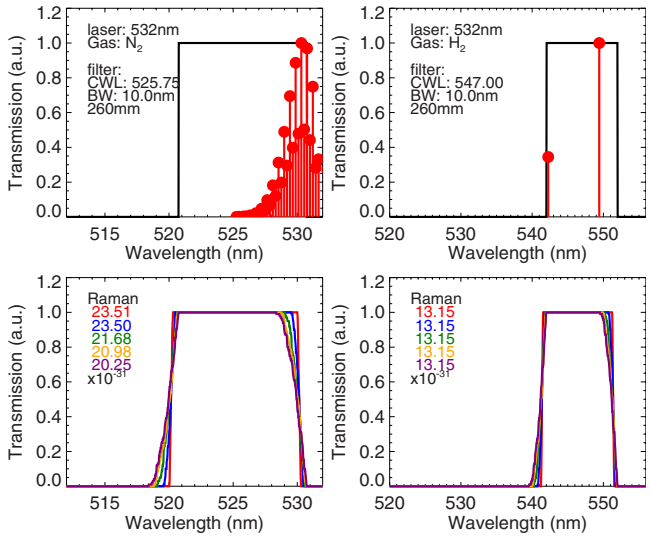

FIG. 7. (Color online) The top plots show the Raman spectra and filter transfer functions for calibrating using a 532 nm laser using N_2 and H_2 gases. The bottom plots show the filter transfer functions shifted by angular variation dependent on the scattering center in the plasma.

spectrum collected by one is compensated by the decrease in spectrum collected by the other. Designing the filters in this manner reduces the susceptibility of the absolute calibration to systematic error.

IX. RAMAN CALIBRATION AT 532 nm

As discussed already the Raman spectrum width increases as λ^2 with increasing wavelength λ. The ability to make optical filters scales linearly with increasing wavelength. Similarly the wavelength shift due to angular variation is a linear function of wavelength. The consequences of these dependencies are that the filter blueshift will become a much more important factor for the accurate detection of Raman scattered signal from a 532 nm laser than from a 1064 nm laser.

This is illustrated by comparison of Fig. 7 for the anti-Stokes nitrogen Raman lines with the equivalent case of a 260 mm filter for a 1064 nm laser in Fig. 4. Both filters have the same wavelength normalized distance from laser wavelength ($\approx 0.25\%\lambda_0$) to provide adequate blocking, and both have identical wavelength normalized bandwidths ($\approx 2\%\lambda_0$). In the case of detecting Raman scattered light from the 1064 nm laser, these specifications result in the filter encompassing a large fraction of the Raman spectrum. That is, the upper cutoff of the bandpass filter is above the peak of the Raman spectrum. In the case of detecting Raman scattered light from the 532 nm laser, these specifications result in the upper cutoff of the bandpass filter being located near the peak intensity of the Raman spectrum. This results in a 20%–25% variation in integrated Raman cross section across the plasma for the filter detecting 532 nm anti-Stokes lines as against a variation of only $\approx 6\%$ for the filter detecting 1064 nm anti-Stokes lines. It is still possible to calibrate using anti-Stokes lines from the 532 nm laser, but great care would have to be taken with the calculation of the filter transmission function to obtain an accurate absolute radial calibration profile.

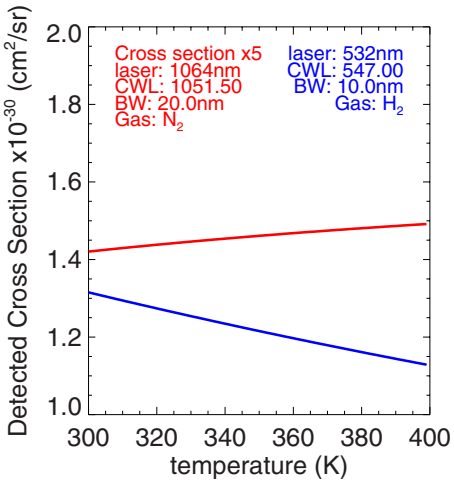

FIG. 8. (Color online) Variation in integrated Raman signal with gas temperature.

Due to the increased size of the shift of the filter relative to the size of the spectrum, calibrating using nitrogen Stokes lines from a 532 nm laser would be difficult. This is particularly the case due to the issue of clearance between the filter and the laser wavelength.

Also shown in Fig. 7 is the possibility of capturing Stokes lines from hydrogen Raman scattering from a 532 nm laser. In this case the separation between Raman lines is large, and the lines are far from the laser wavelength. Hence it is possible to use a filter whose cutoffs are far from the Raman lines. This results in an identical Raman cross section independent of the position of the scattering center in the plasma.

X. TEMPERATURE VARIATION

The sensitivity of the calibration to the temperature of the gas should be minimized as this can introduce systematic uncertainties. The overall uncertainty in the absolute calibration from Raman scattering varies with gas temperature measurement for two reasons. First, the number of gas molecules is a linear function of the measured temperature, as n_{gas} is determined indirectly through a pressure measurement. As a result, the uncertainty in the absolute calibration factor is 0.33% and 0.25% per Kelvin at 300 and 400 K, respectively. Second, the shape of the Raman spectrum is a function of the temperature of the calibrating molecule.

The shape of the Raman spectrum varies with temperature because the fraction of molecules in the *j*th rotation state is determined by the Boltzmann distribution.[10] Figure 8 shows the total detected Raman cross section for two possible scenarios as temperature increases from 300 to 400 K for a fixed gas density. The first is a filter capturing nitrogen anti-Stokes lines from a 1064 nm laser. The second is a filter capturing hydrogen Stokes lines from a 532 nm laser. From this graph it is observed that the systematic in the determined absolute calibration due to change in detected Raman cross section with gas temperature will be approximately +0.1 and −0.2% per Kelvin in these two cases, respectively. This is slightly less than the uncertainty in the number of gas molecules due to the same gas temperature uncertainty for a known pressure of gas.

XI. CONCLUSIONS

Absolute calibration of LIDAR systems can be achieved using a number of different choices of gas and laser wavelength. To minimize the systematic error in this calibration, there should be low variation with plasma radius of the Raman cross section detected by a spectral channel. The combination of nitrogen gas and a 1064 nm laser would work well and is already widely used on current TS systems. In this case, to minimize the variation in integrated Raman cross section with plasma radius, a filter of diameter 260 mm or larger should be used. This diameter would allow a sufficiently sharp filter cutoff to measure to within a few nanometers of the laser wavelength, particularly useful for measurement of Stokes lines. A further interesting possibility is designing filters that collect both Stokes and anti-Stokes lines. This can be done in such a way that changing the angular distribution of light on both filters, the integrated Raman cross section for Stokes and anti-Stokes lines change in opposition, providing greater immunity against systematic error.

For lower laser wavelengths calibration using hydrogenic molecules becomes more attractive. One particular option is calibrating using hydrogen Stokes lines from a 532 nm laser at low gas pressure. The primary benefit of calibrating using a hydrogenic gas is that the Raman lines are far from the laser wavelength and hence far from the filter cutoffs. In this case, the integrated Raman cross section would be invariant with plasma radius. The disadvantage of calibration with hydrogenic gas is the lower scattered signal for a given pressure of gas. This lower signal level could be partially compensated by the significantly greater cross section at lower laser wavelength. The potentially higher detector quantum efficiency at lower wavelength could further increase the detected signal.

ACKNOWLEDGMENTS

This work was funded partly by the United Kingdom Engineering and Physical Sciences Research Council under Grant No. P/G003955 and the European Communities under the contract of Association between Euratom and CCFE. The views and opinions expressed herein do not necessarily reflect those of the European Commission. This work was carried out within the framework of the European Fusion Development Agreement. The authors would also like to acknowledge useful conversations with Mark Kempenaars, Tom Todd, and Roger Huxford.

[1] M. Bassan, L. Giudicotti, and R. Pasqualotto, Appl. Opt. **32**, 5313 (1993).
[2] B. P. LeBlanc, Rev. Sci. Instrum. **79**, 10E737 (2008).
[3] M. J. Walsh, M. Beurskens, P. G. Carolan, M. Gilbert, M. Loughlin, A. W. Morris, V. Riccardo, and Y. Xue, Rev. Sci. Instrum. **77**, 10E525 (2006).
[4] M. Beurskens, L. Giudicotti, M. Kempernaars, R. Scan-nell, and M. Walsh, Rev. Sci. Instrum. **79**, 10E727 (2008).
[5] H. Salzmann, J. Bundgaard, A. Gadd, C. Gowers, K. B. Hansen, K. Hirsch, P. Nielsen, K. Reed, C. Schrödter, and K. Weisberg, Rev. Sci. Instrum. **59**, 1451 (1988).

[6] O. R. P. Smith, C. Gowers, P. Nielsen, and H. Salzmann, Rev. Sci. Instrum. **68**, 725 (1997).
[7] M. Kempenaars, J. C. Flanagan, L. Giudicotti, M. J. Walsh, M. Beurskens, and I. Balboa, Rev. Sci. Instrum. **79**, 10E728 (2008).
[8] L. Giudicotti, R. Pasqualotto, A. Alfier, M. Beurskens, M. Kempenaars, and M. J. Walsh, "Near-Infrared Detectors for ITER LIDAR Thomson Scattering," Nucl. Fusion (submitted).
[9] C. M. Penney, R. L. S. Peters, and M. Lapp, J. Opt. Soc. Am. **64**, 712 (1974).
[10] S. C. McCool, I. L. McCool, R. D. Bengston, and P. E. Phillips "Calibration of Thomson scattering density measurements," Report No. DOE/ET/53042-7, FRCR 234, University of Texas, 1981.
[11] M. V. de Sande, Ph.D. thesis, Technische Universiteit Eindhoven, Eindhoven, The Netherlands, 2002.
[12] G. Vaughan, D. P. Wareing, S. J. Pepler, L. Thomas, and V. Mitev, Appl. Opt. **32**, 2758 (1993).
[13] H. Röhr, Phys. Lett. A **81**, 451 (1981).
[14] G. Herzberg, *Molecular Spectra and Molecular Structure*, Spectra of Diatomic Molecules, Vol. 1, 2nd ed. (Van Nostrand, New York, 1950).
[15] R. Scannell, M. Walsh, P. G. Carolan, A. C. Darke, M. R. Dunstan, R. B. Huxford, G. McArdle, D. Morgan, G. Naylor, T. O'Gorman, S. Shibaev, N. Barratt, K. J. Gibson, G. J. Tallents, and H. R. Wilson, Rev. Sci. Instrum. **79**, 10E730 (2008).